

A multimodality vascular imaging phantom of an abdominal aortic aneurysm with a visible thrombus

Louise Allard

Laboratory of Biorheology and Medical Ultrasonics, Research Center,
University of Montreal Hospital (CRCHUM), Québec H2L 2W5, Canada

Gilles Soulez

Department of Radiology, University of Montreal Hospital (CHUM), Québec H2L 2M1, Canada;
Department of Radiology, Radio-Oncology and Nuclear Medicine, University of Montreal,
Québec H3T 1J4, Canada; and Institute of Biomedical Engineering, University of Montreal,
Québec H3T 1J4, Canada

Boris Chayer and Zhao Qin

Laboratory of Biorheology and Medical Ultrasonics, Research Center,
University of Montreal Hospital (CRCHUM), Québec H2L 2W5, Canada

David Roy

Institute of Biomedical Engineering, University of Montreal, Québec H3T 1J4, Canada

Guy Cloutier^{a)}

Laboratory of Biorheology and Medical Ultrasonics, Research Center, University of Montreal Hospital
(CRCHUM), Québec H2L 2W5, Canada; Department of Radiology, Radio-Oncology and Nuclear Medicine,
University of Montreal, Québec H3T 1J4, Canada; and Institute of Biomedical Engineering,
University of Montreal, Québec H3T 1J4, Canada

(Received 4 December 2012; revised 11 April 2013; accepted for publication 12 April 2013;
published 14 May 2013)

Purpose: With the continuous development of new stent grafts and implantation techniques, it has now become technically feasible to treat abdominal aortic aneurysms (AAA) with challenging anatomy using endovascular repair with standard, fenestrated, or branched stent-grafts. *In vitro* experimentations are very useful to improve stent-graft design and conformability or imaging guidance for stent-graft delivery or follow-up. Vascular replicas also help to better understand the limitation of endovascular approaches in challenging anatomy and possibly improve surgical planning or training by practicing high risk clinical procedures in the laboratory to improve outcomes in the operating room. Most AAA phantoms available have a very basic anatomy, which is not representative of the clinical reality. This paper presents a method of fabrication of a realistic AAA phantom with a visible thrombus, as well as some mechanical properties characterizing such phantom.

Methods: A realistic AAA geometry replica of a real patient anatomy taken from a multidetector computed tomography (CT) scan was manufactured. To demonstrate the multimodality imaging capability of this new phantom with a thrombus visible in magnetic resonance (MR) angiography, CT angiography (CTA), digital subtraction angiography (DSA), and ultrasound, image acquisitions with all these modalities were performed by using standard clinical protocols. Potential use of this phantom for stent deployment was also tested. A rheometer allowed defining hyperelastic and viscoelastic properties of phantom materials.

Results: MR imaging measurements of SNR and CNR values on T1 and T2-weighted sequences and MR angiography indicated reasonable agreement with published values of AAA thrombus and abdominal components *in vivo*. X-ray absorption also lay within normal ranges of AAA patients and was representative of findings observed on CTA, fluoroscopy, and DSA. Ultrasound propagation speeds for developed materials were also in concordance with the literature for vascular and abdominal tissues.

Conclusions: The mimicked abdominal tissues, AAA wall, and surrounding thrombus were developed to match imaging features of *in vivo* MR, CT, and ultrasound examinations. This phantom should be of value for image calibration, segmentation, and testing of endovascular devices for AAA endovascular repair. © 2013 American Association of Physicists in Medicine. [<http://dx.doi.org/10.1118/1.4803497>]

Key words: vascular flow phantom, abdominal aortic aneurysm, thrombus, medical imaging, medical physics

I. INTRODUCTION

Abdominal aortic aneurysm (AAA) can be defined as a progressive enlargement of the aorta leading to its potential rupture. The risk of rupture is clinically determined by the rate of increase of the AAA and by its maximal diameter.¹ Usually, preventing treatment is indicated for asymptomatic AAA measuring more than 50 mm in diameter. Even though surgical repair of an aneurysmal segment by a vascular graft is a standard procedure, endovascular aneurysm repair (EVAR) is a promising less invasive alternative with reduced rates of immediate mortality/morbidity and a more rapid recovery than open surgery for patients.²⁻⁵ The main limitations of EVAR are the occurrence of an incomplete seal of the endovascular graft (endoleak) or persistent pressurization of the aneurysm sac without blood flow in the sac (endotension).^{6,7}

The success of EVAR depends on reliable baseline assessment of anatomy, appropriate selection of the endograft, and sensitive postdeployment imaging monitoring of the graft for complication detection.⁸ Patients with a short or angulated proximal neck, the presence of thrombus atheroma or severe calcification in the neck, and tortuous or small iliac arteries are not eligible for EVAR.^{9,10} With the continuous development of new stent grafts and implantation techniques, it has now become technically feasible to treat AAAs with challenging anatomy, especially short and angulated necks. Such procedures are possible with suprarenal fixation, and fenestrated and branched stent grafts to preserve the patency of renal or visceral arteries.

Experimental and numerical studies of EVAR are in development to investigate endoleaks and endotensions providing relevant information for the development of new stent-graft designs but up to now they are not validated.¹¹ Among others, *in vivo* animal experimentations have played an important role in the understanding of the mechanisms underlying the development of AAAs and are still an interesting means for validating new endovascular techniques.^{12,13} Animal experimentations have also been relevant to human diseases by giving more detailed information on the healing process following EVAR and the genesis of endoleaks.^{14,15} These animal models are expensive, difficult to control or repeat, and measurement accuracy cannot always be precisely determined.¹⁶ Furthermore, animal lesions do not adequately simulate the complex 3D anatomy and, in particular, the thrombus frequently observed in large human AAAs.¹⁵ Also, the stent must often be downsized to fit animal vessels, which are smaller than human ones.¹⁷

On the other hand, *in vitro* experimentations are very useful in the development phases of stent grafts and in improving implantation techniques. In vascular replicas, the knowledge of the shape of the simulated vessel is helpful to understand the impact of the surgical anatomy on stent-graft delivery and conformability, and can simulate high-risk clinical procedures to improve outcome.¹⁶ Furthermore, since advanced guidance in the angiographic suite involves registration of several imaging modalities, vascular phantoms compatible with these different modalities are very helpful to validate the accuracy of multimodal registration and segmentation methods.¹⁸

They are also useful to evaluate image artifacts produced by endovascular metallic devices¹⁹ and in hemodynamic flow studies.²⁰ However, most AAA phantoms available are simple and not physiologically shaped while others only mimic the lumen or the external wall of the artery.^{16,21-23} Some others represented the intraluminal thrombus by simply thickening the external wall of the mimicked artery.^{17,24,25}

It is well known that intraluminal thrombus may reduce aneurysm wall shear stress^{26,27} and that the size of the thrombus provides different protection against rupture.^{26,28} Thrombus extension especially in the vicinity of landing zones impacts patient and stent-graft selection.¹⁷ It is, thus, important that the vascular phantom represents accurately the lumen and the thrombus for both stent-graft implementation and flow studies. Hence, there is a real need for realistic *in vitro* models for evaluating endovascular techniques, testing new endovascular materials, and for training purposes ahead of *in vivo* studies. The purpose of this study was to develop a realistic complex geometry of an AAA with a vascular lumen and a distinct thrombus having similar imaging properties than human's one in magnetic resonance angiography (MRA), computed tomography angiography (CTA), digital subtraction angiography (DSA), and ultrasound (US).

II. MATERIALS AND METHODS

II.A. Image processing and rapid prototyping

The molded realistic AAA geometry was a replica of a multidetector computed tomography (MDCT) scan taken from a patient with an AAA before undergoing surgery. The scanning parameters were the following: pitch 1, slice thickness 1 mm, collimation 0.75, and viewing field 300 (Somatom Sensation 16, Siemens, Erlangen, Germany). The examination was performed with intravenous contrast at 4 ml/s for a total of 100 ml.

To recover the 3D geometry, the outer arterial wall and the luminal boundary were manually segmented with SliceOmatic (version 4.2, TomoVision Inc., Montreal, QC, Canada) by considering the image gradient. The 3D model was transferred into PolyWorks (version 8.1, InnovMetric Inc., Quebec City, QC, Canada) to smooth and resample the contours and to produce output files compatible with stereolithography [Figs. 1(a) and 1(b)]. Two epoxy resin skeletons representing the smoothed surface of the lumen and the lumen with the thrombus [Figs. 1(c) and 1(d)] were generated by stereolithography (Dorval Technologies, Montreal, QC, Canada). These positives were then used to create the master silicone molds (i.e., negative molds) to cast the replicas of the lumen and AAA thrombus.

II.B. Design of the vascular wall and vessel lumen

The lost-material casting method was based on isomalt,²⁹ which is a commercial sugar polyalcohol widely used as a sweetener. It was melt at a temperature between 145 °C and 150 °C and poured into a two-part silicone mold to reproduce the shape of the lumen. After casting, the isomalt core was cooled at room temperature for 2 h. It was then extracted from

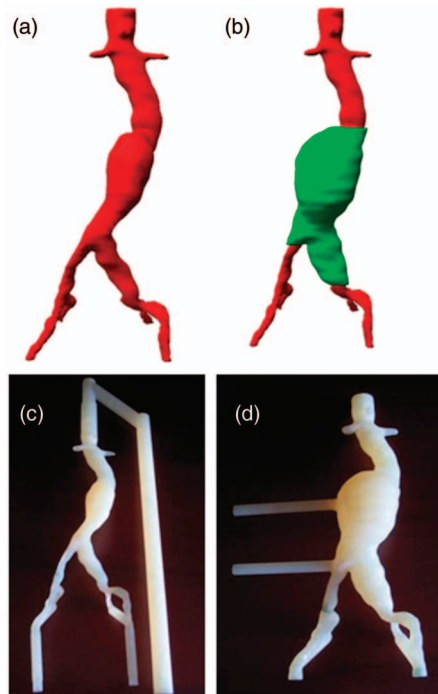


FIG. 1. Stereolithography compatible input images of the lumen (a) and lumen with the thrombus (b) sent to the stereolithography process to create epoxy resin skeletons representing the lumen (c) and lumen with the thrombus (d). The skeletons in (c) and (d) were used to create the master silicone molds of the AAA geometry; the holders on the resin skeletons were removed from the silicone molds. Note that the iliac bifurcations were artificially jointed together for attachment to a single connector of the phantom.

the mold and slightly hand-polished to remove unavoidable residues at the mold junctions. The diameter of the proximal neck of the AAA was estimated at 22.7 mm, while the AAA larger luminal diameter was 38.5 mm. To avoid diffusion of contrast material during imaging (typically gadolinium in MRA or iodine in CTA and DSA), a thin membrane of liquid polyurethane (product number ren-6400-1, Huntsman International, Mississauga, ON, Canada) was uniformly painted onto the surface of the isomalt core (dark for black and white display in Fig. 2). Time was allowed for the drying of polyurethane before surrounding it with a gel mimicking the AAA thrombus (white upstream of the bifurcation in Fig. 2).

II.C. Design of the gel mimicking thrombus

For a typical volume of 500 ml, the gel mimicking the AAA thrombus was made of a mixture of 35 g of agar (number A-6924, Sigma Chemical, St-Louis, MO), 20 g of glycerol (number G-5516, Sigma Chemical), 0.5 g of sodium azide to prevent bacterial growth (number S-2002, Sigma Chemical), 15 g of cellulose particles (Sigmacell, number S-5504, Sigma Chemical), and 430 ml of distilled water. The mixture was heated at 60 °C and stirred to get a homogeneous gel. The isomalt core painted with the thin polyurethane layer representing the wall of the aorta was placed into the second silicone mold. The gel mixture was then poured into the mold to obtain the thrombus. The maximum AAA diameter (lumen

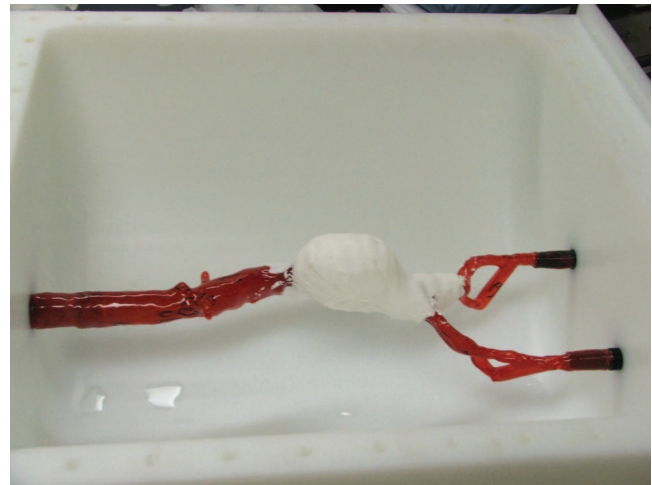


FIG. 2. AAA phantom with the isomalt core painted with polyurethane (in dark for black and white display) used to create the lumen and thrombus (upstream of the bifurcation) before pouring the mimicking agar-oil gel of the abdomen within the polyethylene container.

+ thrombus) was 51 mm. Time was allowed for the solidification of the gel before demolding.

II.D. Process for manufacturing the vascular phantom

As illustrated in Fig. 2, the AAA phantom was enclosed in a polyethylene container, the inner of it having a semicylindrical shape surrounding the vessel geometry. The 42-cm diameter of the semicylindrical cavity was similar to a typical human adult abdomen and its length was 50 cm. The next step of the fabrication process relied on introducing the cast of the lumen with thrombus into the phantom container that included connectors for a tubing system made of one inflow at the proximal portion of the aorta and two outflows, one for each iliac artery (Fig. 2). The use of external tubing enabled filling the AAA lumen with contrast agent for imaging or with a mimicking fluid for flow circulation experiments, if desired.

Then, a first layer of a mixture of agar-paraffin gel was poured into the phantom and 72 spherical markers were implanted at precise known positions in that layer of gel, according to the manufacturing process described previously.³⁰ These fiducial markers can be used for calibration, rescaling, and fusion of 3D images obtained from these different modalities, and 3D image reconstruction from angiographic plane views. Markers were inserted at controlled angular positions and a depth of 3 mm from the bottom cylindrical surface of the phantom. They were divided in eight sets of nine markers each. For each set, the glass balls of 3-mm diameter were contained in nonsymmetrical cross-sectional and longitudinal planes to facilitate image localization. For the same reason, in each cross-sectional planar set, the beads were implanted at different angular positions on either side of the cylindrical symmetry axis. A period of 3 h was allowed for the solidification of the first layer of gel. As reported by Cloutier *et al.*,³⁰ the use of paraffin oil (number 06712029, Fisher Scientific, Fairlawn, NJ) in that layer of gel allows glass balls to be visible in MRA. Those balls were also distinguishable on CTA, DSA, and US images.

A second layer of gel was designed to have similar imaging properties as an average human abdomen in MRA, CTA, DSA, and US examinations. Twenty-three liters of a mixture gel were prepared, 1 liter at a time, by using for each liter 32 g of agar, 2 g of glucosamine (D-glucosamine 6-sulfate, number G-8641, Sigma Chemical) to stabilize the emulsion, 1 g of sodium azide, 214 ml of paraffin oil, and 788 ml of distilled water. Each liter of the mixture was prepared separately and stirred until the gel-oil emulsion became homogeneous, i.e., until the water and oil did not separate after stirring. Then, 23 liter of gel were stirred all together and heated at 60 °C during 15 h before being poured into the phantom to fill the container up to the cover made of a polyethylene sheet. To avoid drying out of the agar-oil gel, a rubber gasket was installed between the cover and the container. A thin layer of water was introduced between the second layer of the gel and the polyethylene cover to avoid air trapping and to ensure acoustic coupling for US measurements.

To create the vessel lumen, the phantom was submerged in a water bath, at room temperature, for several hours. As the water got in contact with isomalt through the tubing system, it started dissolving out of the phantom via the plastic tubes. At the end, a conduit with a polyurethane wall having the shape of the isomalt luminal cast was produced, surrounded by the simulated AAA thrombus and gel mixture mimicking abdominal tissues.

II.E. Mechanical testing of (static) hyperelastic phantom materials and density measurements

Mechanical tests were done with specimen samples as per Brown,³¹ i.e., of cylindrical shape (diameter of 25 mm, thickness of 5 mm) and were conducted in a rheometer (Anton Paar "Physica MCR 501", Graz, Austria). Shear strain (static) tests were conducted to assess the limit of rupture in terms of shear stress. Three specimen samples were used for every static test, namely, for the agar-oil gel mimicking abdominal tissues, the agar-glycerol gel simulating the thrombus, and the polyurethane mimicking the AAA vascular wall. All specimen samples were undergoing a vertical force of 4 N, in order to simulate average physiological conditions (i.e., weight of surrounding soft tissues and blood pressure). Materials were also poured into small vials for density measurements.

II.F. Image acquisitions

To demonstrate the multimodality imaging capability of the new AAA phantom (i.e., with fiducial markers and a thrombus visible in MRA, CTA, DSA, and US), image acquisitions were performed by using standard clinical protocols. Multimodality image acquisitions were performed at room temperature and no flow was circulating in the phantom (static condition).

II.F.1. MR-angiography

MRA imaging was performed with a 1.5 T unit (Avanto, Siemens, Erlangen, Germany). The phantom was first filled

with serum saline and imaged using a body array coil with the following axial and coronal T1 weighted spin echo (SE) sequences: repetition time (TR) = 574 ms, echo time (TE) = 13 ms, flip angle (FA) = 180°, and voxel size = 1.2 × 0.6 × 5 mm. Then axial and coronal T2 fast spin echo (FSE) sequences were acquired with TR = 4030 ms, TE = 115 ms, FA = 180°, and voxel size = 1.2 × 0.6 × 5 mm. The phantom vessel was filled with 9 ml of 0.5 mole/l gadopentetate dimeglumine solution (Prohance, Bracco Diagnostics, Princeton, NJ) diluted in 250 ml of 0.9% NaCl solution giving a 1.8 mmole/l concentration. The same axial and coronal T1 weighted acquisitions were repeated. Then, a high resolution three-dimensional fast low angle shot (FLASH) gradient echo (GE) sequence in the coronal plane was acquired (TR = 3.2 ms, TE = 1.1 ms, FA = 20°, voxel size = 1.0 × 0.7 × 1.2 mm). For each sequence, the region of interest (ROI) was taken for signal intensity measurement in the lumen, agar-glycerol thrombus, agar-oil mimicked abdomen, agar-oil peripheral layer containing fiducial markers, and outside the phantom to calculate the following parameters: signal-to-noise ratio (SNR) = mean signal/standard deviation of the background noise and contrast-to-noise ratio (CNR) = SNRA - SNRB, where A and B are two different ROIs within the image.

II.F.2. CT-angiography

For CTA, the aortic lumen was filled with a 2.8% v/v (volume concentration) solution of 430 mg/ml iohalamate meglumine (Conray 43, Mallinckrodt Medical, Pointe-Claire, QC, Canada) diluted in a 0.9% NaCl solution. The phantom was imaged with a Somatom Sensation 64-slice scanner (Siemens, Erlangen, Germany) by using a collimation of 64 × 0.6 mm, a pitch of 0.45, a rotation time of 0.37 s, a slice thickness of 1 mm, and a reconstruction interval of 0.7 mm. Acquisition parameters were a current intensity of 217 mA, a peak voltage of 120 kV, a matrix size of 512 × 512, and a field of view of 38 cm. Then, 3 mm coronal and sagittal multiplanar reformations (MPR) and maximal intensity projections (MIP) were generated. ROIs were drawn in the lumen with and without contrast, agar-glycerol thrombus, agar-oil abdominal gel, and agar-oil peripheral fatty layer to measure the density in Hounsfield unit (HU) of the main phantom components.

II.F.3. X-ray angiography

In DSA, the phantom was filled with a contrast solution of iohalamate meglumine at 141 mg/ml (Conray 30, Mallinckrodt Medical, Pointe-Claire, QC, Canada). Digital spot film acquisitions at 0° and 45° RAO (right-anterior-oblique) and LAO (left-anterior-oblique) projections were performed on an Axiom Artis dTA unit (Siemens, Forchheim, Germany) by using the following parameters: field-of-view = 32 cm, tube-intensifier distance = 100 cm, table height = 80 cm, matrix size = 1024 × 1024, current intensity = 400 mA, and peak voltage = 70 kV.

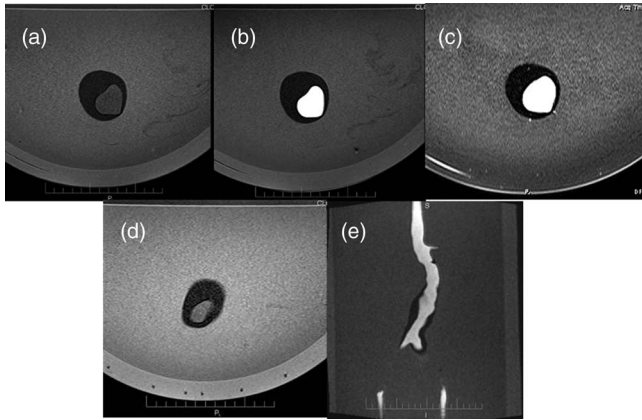


FIG. 3. MRA examination of the phantom. (a) T1 weighted spin echo sequence without contrast, (b) T1 weighted spin echo sequence with contrast, and (c) T2 weighted sequence without contrast. The differentiation between the lumen, the thrombus, and the agar-oil abdominal gel is well demonstrated on all acquisitions and signal intensities are similar to those observed clinically. (d) T1 weighted spin echo sequence, showing a plane with visible fiducial markers in the peripheral fatty layer (hyposignal intensity). (e) T1 weighted 3D FLASH gradient echo sequence with contrast injection. The lumen, thrombus, agar-oil abdominal gel, and peripheral fatty layer can still be differentiated. No clinical MRA examination of the patient used as a model to build this phantom was available for comparison.

II.F.4. Ultrasound

Finally, a Vivid Five ultrasound scanner (General Electric Medical Systems, Milwaukee, WI) with a 192-element linear array probe (FLA 10 MHz) was used to collect B-mode cross-sectional images. The vessel lumen was filled with degassed water to allow US transmission. Acoustic velocities of the agar-glycerol mimicked thrombus and agar-oil gel simulating the abdominal tissue of the phantom were measured using a pulse transit time technique, similar to that described by Madsen *et al.*³² The experimental method is described in Cloutier *et al.*³⁰

II.G. Stent deployment and fluoroscopy

To demonstrate the technical feasibility of a stent deployment in our AAA phantom, a bifurcated abdominal aortic

stent graft (28 mm diameter bifurcated main body graft, 10 mm diameter ipsilateral, and 12 mm diameter contralateral iliac legs, Zenith Cook Medical, Bloomington, IN) was inserted through the right iliac connector of the phantom for the main body and the left iliac connector for the left iliac limb. The delivery systems (22 French introducer for the main body and 16 French for the left iliac) were introduced along a 0.035 mm stiff guide wire (Lunderquist, Cook Medical, Bloomington, IN) under fluoroscopic guidance and stents were deployed as recommended in the instruction for use.

III. RESULTS

III.A. The AAA phantom with a thrombus

Figures 3–6 provide opportunities to judge the quality of the representation of the AAA phantom in different modalities and the visibility of fiducial markers when present in the imaging plane. Figures 4 and 6 also allow comparing these representations with the US and CTA exams of the patient that served as a model for this AAA phantom. In MRA (Fig. 3), the thrombus area was hypointense in T1 and T2 weighted SE sequences, and T1 weighted FLASH-GE sequence. It could be differentiated on each sequence from the lumen without contrast on T1 and T2 weighted SE sequences, and with contrast on T1 weighted SE and T1 weighted FLASH-GE sequences. Since no flow was circulated in the phantom, only the lumen signal of the T1 weighted FLASH-GE sequence was representative of the clinical reality. SNR and CNR values of the different components of the phantom are detailed in Tables I and II.

In CTA (Fig. 4), the thrombus presented a higher density (25 HU) than the agar-oil gel mimicking the abdominal tissue and fat (–28 HU). The peripheral agar-oil layer of the phantom was more hypodense (–38 HU). Fiducial markers did not produce image artifacts and were well delineated on axial and coronal reformations and MIP. After contrast enhancement, the lumen density was estimated at 120 HU. In order to compare CT imaging features of the phantom with real patient data, we measured on the original clinical CT of the selected patient for AAA prototyping, the following densities in HU: (1) the most hyperdense and hypodense portions

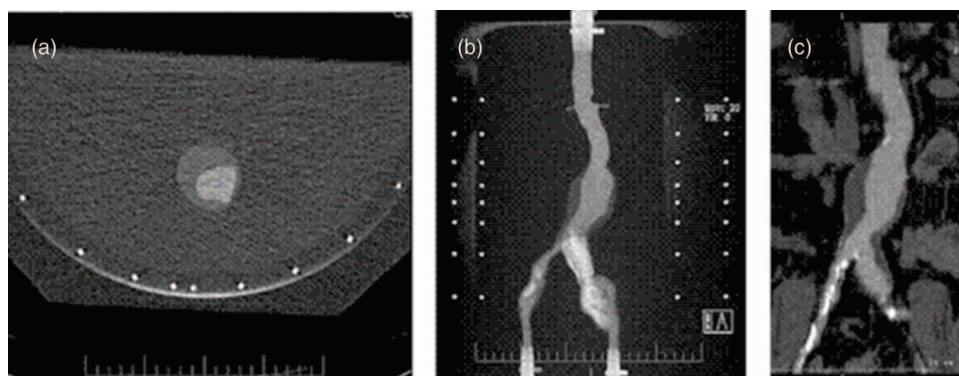


FIG. 4. (a) Axial CTA scan acquisition showing the thrombus with a slightly higher density than the surrounding agar-oil gel of the abdomen and a strong enhancement of the lumen by the contrast agent. (b) Coronal acquisition showing the differentiation between the lumen, the thrombus, and the surrounding tissue. Fiducial markers are well delineated in both panels. (c) Coronal acquisition of the patient used as a model to build this phantom.

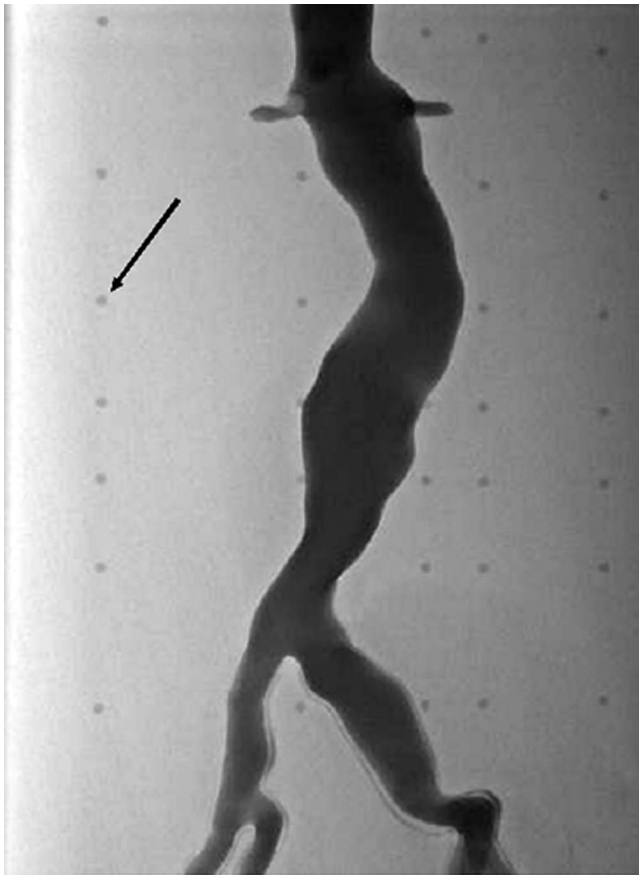


FIG. 5. Digital spot film acquired with the DSA unit showing the lumen of the AAA and fiducial markers in the background (arrow). No clinical DSA examination of the patient used as a model to build this phantom was available for comparison.

of the AAA thrombus, (2) AAA lumen, (3) retroperitoneal fat, and (4) psoas muscle and small bowel. All these measurements have been taken before and after iodine contrast injection (Table III). In angiography (Fig. 5), only the lumen filled with contrast was seen and fiducial markers were well observable in the background of the image.

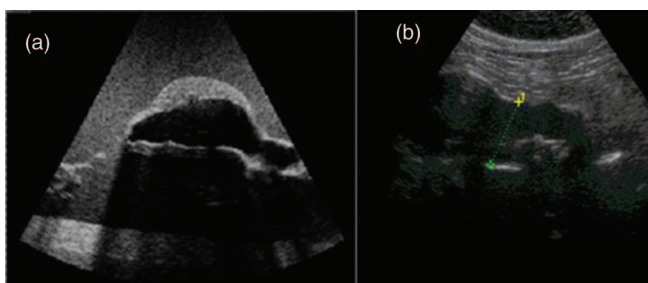


FIG. 6. (a) Ultrasound B-mode image showing a longitudinal view of the lumen and thrombus of the AAA. A strong attenuation of the echo signal is seen at the bottom of the image. This is due to the thick layer of polyurethane that was used to prevent puncture of the vessel wall when deploying the stent-graft; this is a requirement that we did not have to consider in the previous art (see Refs. 29 and 30). (b) Longitudinal ultrasound acquisition of the patient AAA used as a model to build this phantom.

TABLE I. SNR values of the different components of the AAA phantom (lumen, thrombus, mimicked abdomen, and fatty layer embedding glass ball markers).

SNR	Thrombus	Abdomen	Fatty layer	Glass balls
T1 SE	49.6	91.8	108.1	66.2
T2 SE	6.3	15.1	12.0	7.0
FLASH-GE	2.6	8.3	28.1	23.2

In US imaging (Fig. 6), the lumen, the thrombus, and fiducial markers (not seen on this example) were visible. The propagation speeds within the agar-oil gel of the mimicked abdomen (1458 m/s) and that of the agar-glycerol AAA thrombus (1493 m/s) were similar to reported values of biological tissues.³³ Shadowing artifact is seen at the bottom of the image.

III.B. Stent deployment

The procedure was technically successful. The guide wires, catheter, delivery catheters, and stent-graft components were easily inserted into the phantom through the iliac limbs and well tracked under fluoroscopic guidance. Angiography images of the stented aortic phantom showed the full deployment of the graft and of its iliac branches (Fig. 7). *A priori* knowing the exact 3D geometry of the vessel lumen allowed to choose the appropriate stent configuration.

III.C. Mechanical properties and densities

The three major constitutive materials of the phantom, i.e., agar-oil mixture of the abdomen, agar-glycerol thrombus gel, and polyurethane vessel wall were found to have hyperelastic stress-strain curves with a logarithmic shape (Figs. 8–10), while real biological tissues such as bowels and arteries are characterized by exponentially shaped hyperelastic stress-strain relations,³⁴ and real thrombi present an almost linear elastic behavior.³⁵ Therefore, we cannot directly compare tested “close viscoelastic” mimicking materials with “stiffening hyperelastic” and “linear elastic” biologic materials. Indeed, biological tissues that exhibit a stiffening nonlinear behavior, mainly due to collagen fibers, are not easy to replace with artificial substitutes.

Densities of the mimicking structures used for the thrombus and the surrounding materials were measured at 1.04 mg/cc for the thrombus, 0.98 mg/cc for the surrounding gel, and 1.04 mg/cc for the polyurethane wall.

TABLE II. CNR values of the different components of the AAA phantom.

CNR	Thrombus/abdomen	Abdomen/fat layer	Fat layer/glass balls
T1 SE	− 42.2	− 16.3	41.9
T2 SE	− 8.8	3.1	5.0
FLASH-GE	− 5.7	− 19.8	4.8

TABLE III. Clinical values (HU) obtained from the CTA of the patient used as a model for our AAA phantom.

	Unenhanced CT	Enhanced CT
Aortic lumen	53	250
Hyperdense thrombus	60	63
Hypodense thrombus	50	44
Retroperitoneal fat	- 101	- 99
Psoas muscle	68	55
Small bowel	44	87

IV. DISCUSSION

IV.A. Design challenges

The development of a new patient specific AAA phantom with a thrombus was a great challenge considering the physics of each imaging modality (MRA, CTA, DSA, and US) and the choice of the materials needed to mimic clinical image features of the lumen, thrombus, and abdominal surrounding tissues. Indeed, besides the choice of the appropriate concentration of agar, water, and other compounds (paraffin oil, cellulose particles, polyurethane) to confer proper imaging properties, this composition had to be molded and to permit stability over time. Several empirical tests had to be realized to get the best compromise between MR relaxation times, x-ray absorption, and speed of sound. Few groups



FIG. 7. CTA image showing a stent graft deployed into the lumen of the AAA phantom and a visible thrombus. Fiducial markers are seen in the background of the image.

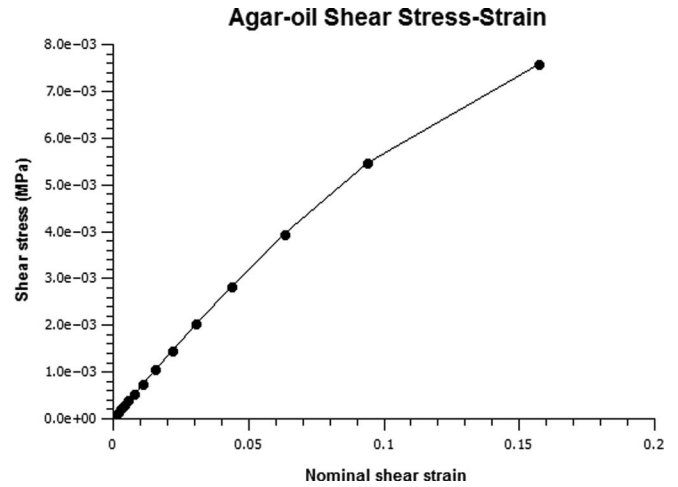


FIG. 8. Shear stress τ as a function of applied shear strain Υ for the agar-oil gel mimicking the abdominal aorta.

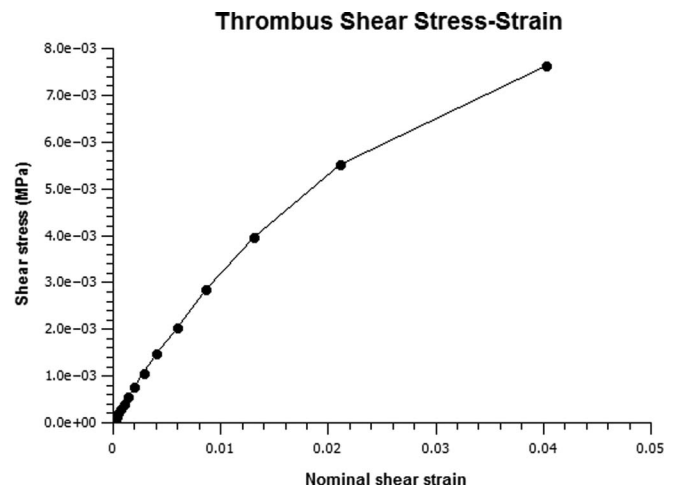


FIG. 9. Shear stress τ as a function of applied shear strain Υ for the agar-glycerol gel mimicking the thrombus.

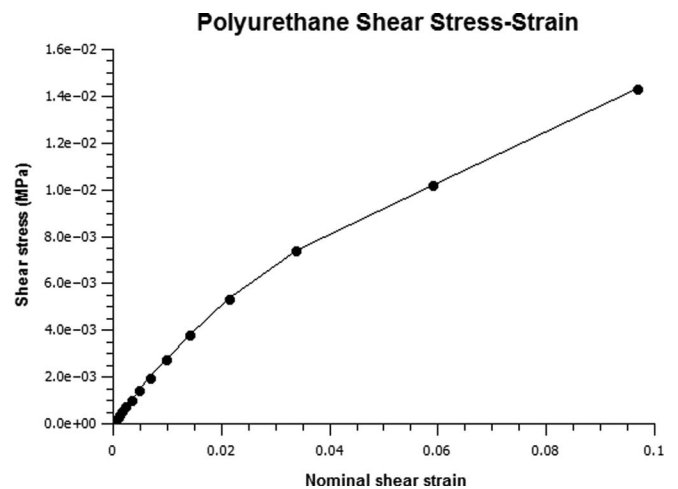


FIG. 10. Shear stress τ as a function of applied shear strain Υ for the polyurethane mimicking the vessel wall.

who developed multimodality phantoms had to deal with these disparities inherent to each modality. Frayne *et al.*³⁶ used polyester resin for their vessel wall. This relatively poor tissue mimicking material created artifacts in US and truncation artifact in MRI. Moreover, Dabrowski *et al.*³⁷ used stainless steel ball bearings as fiducial markers. These created artifacts in US and CT and could not be used in MRI. Note that in the proposed vascular phantom, the tissue mimicking agar-based gels is isotropic and homogenous while in patients, the abdominal aorta is surrounded by bone structures, by retroperitoneal fat, and structures with different tissue densities (e.g., psoas muscle, bowel, etc.). Thus, the heterogeneous nature of the abdomen could not be considered in the current design nor were realistic mechanical properties of the different structures. Nevertheless, an important feature of this phantom for calibration and image registration purposes is the visibility of image markers in all modalities. As reported earlier,³⁰ this was another important challenge to consider.

The relative hyposignal observed in the simulated thrombus on T1 that was more pronounced on T2-weighted spin echo sequences is in accordance with clinical observations of organized thrombus in AAA patients.^{38,39} Kramer *et al.*⁴⁰ reported in AAA patients SNR values of 16 in organized thrombi on EKG-gated T1-weighted spin echo sequences. This SNR is lower than the value of 50 reported in our study. However, since with EKG gating the TR value depends on the RR wave interval, the weighting was probably between T1 and T2 explaining a lower signal in this clinical situation. On T2-weighted sequence, SNR values are in good concordance with those reported by Kramer *et al.*⁴⁰ (13 versus 6). The SNR values of the simulated abdomen and peripheral fat on T1 weighted sequence were also realistic with a hyperintense signal less pronounced on the abdominal than the fat layer component, similar to retroperitoneal and abdominal fats and subcutaneous adipose tissues. The signal decrease of the simulated abdomen on T2-weighted spin echo sequence was also typical of clinical observations. This was confirmed by higher absolute CNR values between the thrombus and the abdomen, and the abdomen and the fat layer on T1-weighted spin echo sequence, as compared with the T2-weighted sequence. Finally, the more hyperintense signal in the peripheral fat layer was helpful to discriminate the fiducial markers on T1-weighted sequences, as shown by the SNR value of 66.

The thrombus was homogeneous whereas 47% of AAA patients present areas of higher signals on T1 and T2 due to the presence of nonorganized thrombus.⁴¹ This can be a limitation but it is difficult to recreate all the variability associated with the thrombus maturation *in vitro*. Regarding the AAA lumen, since the phantom was not connected to a pump for flow circulation in acquired MR images, the luminal signal observed in our experiments was different from that of a real patient on T1 and T2 weighted SE sequences, where a flow void is expected because of proton dephasing. Nevertheless, we could differentiate the different parts of the phantom on tested MR sequences and a strong hypersignal was found on GE-enhanced T1 weighted gradient acquisition, as observed in real patients.

CT densities observed for the patient and our phantom were quite similar. Indeed, as shown in Table III, *in vivo* thrombus densities ranged between 44 and 63 HU, whereas our phantom thrombus was measured at 25 HU. The retroperitoneal fat was evaluated between -101 and -99 *in vivo*, whereas the peripheral layer of the phantom was measured at -38 . Finally, psoas and small bowel density values ranged between 44 and 87 HU for the patient. The value of agar gel around the AAA was evaluated at -30 HU. Since the abdominal compartment is made of abdominal/retroperitoneal fat mixed with bowels and retroperitoneal muscle, this value is a good compromise between fat and other tissue densities. The HU values in CTA for the surrounding abdomen material (-28 HU) and the thrombus (25 HU) are in reasonably good agreement with clinical values obtained for the patient (Table III) and values cited in the literature considering that the contrast between both tissues can be modulated by varying the window width of the ROI.⁴² Yoshizumi *et al.*⁴³ estimated the mean distribution of the abdominal fat at -92 HU. D'Souza *et al.*⁴⁴ mentioned that HU numbers for most soft tissues (excluding fat) lie in the range of 20–90, while Tokunaga and Hanaizumi⁴⁵ noted that HU values of AAA thrombi range from 50 to 270, according to its structural organization. On the other hand, Tomoda *et al.*,⁴⁶ in a case study, obtained a HU number of 68 for the thrombus. Roy *et al.*⁴⁷ observed that area of hyperdensity can be observed in the thrombus and wall of ruptured aneurysm due to the presence of intramural hematoma.

To avoid image distortion in US imaging, Madsen *et al.*³² suggested the use of mimicking tissues with speeds of sound ranging from 1460 to 1640 m/s. The current study revealed values of 1493 m/s for the mimicked thrombus and 1458 m/s for the simulated abdomen. Bullen *et al.*⁴⁸ mentioned that the subcutaneous fat has a propagation speed of 1476 m/s. Muscles and soft tissues such as the liver are characterized by speeds of sound ranging from 1540 to 1600 m/s.⁴² The propagation speed varies in AAA artery wall according to the organization of the thrombus (associated with levels of collagen and cholesterol).⁴⁹ These authors obtained a mean speed of sound of 2000 m/s for calcified arteries. According to the literature,⁵⁰ the speed of sound for the selected polyurethane mimicking the artery wall in our study was 1500 m/s. We can, thus, conclude that selected materials provided acceptable representation of real AAAs and surrounding biological tissues. As noticed in Fig. 6, the shadowing observed at the bottom of the image was due to the combined attenuation of the different materials.

IV.B. Mechanical properties in the context of an endovascular intervention

Previous *in vitro* studies reported that the most important components of any AAA phantoms are its reproducibility, consistency of material properties and thicknesses, and mechanical behavior (i.e., stiffness and compliance).^{51–54} While our phantom provides a good representation of the clinical reality from geometric and imaging standpoints, aspects that are innovative, further investigation would be needed to define

adequate materials representing nonlinear viscoelastic properties of real AAAs. As mentioned by Corbett *et al.*,⁵⁴ because the abdominal aorta is surrounded by visceral organs, abdominal muscles, and the spine, it is difficult to reproduce *in vitro* a model that would mechanically behave as *in vivo*. However, we believe our model could fairly represent the linear mechanical behavior of soft tissues in the physiological range of—relatively small—deformations, as it is reflected by the satisfying correlation we obtained from an imaging standpoint (based on linear mechanical properties, i.e., elasticity moduli). Obviously, a thorough comparison of vasculature deformation based on *in vivo* studies/data is still needed for the sake of validation.

The imaging compatibility with all modalities is relevant to optimize new endovascular techniques of stent-graft implementation (fenestrated or branched stent-grafts), and to validate new techniques of 2D/3D fusion between DSA and cone-beam CT, and potentially between intravascular US and DSA. Although we could efficiently release an endovascular stent graft in the phantom, the current prototype could be inaccurate to simulate the geometric deformation occurring during AAA endovascular repair because mechanical properties of the AAA phantom did not reflect the complexity of biological tissues. This is likely to happen since EVAR involves large deformations and rotations of the vascular structure and its surrounding medium, especially for the iliac arteries. Therefore, it is absolutely necessary to conduct *in vivo* studies to capture the real complex mechanical response of the abdominal region, which would ensure a realistic phantom design. In this regard, Demirci *et al.*⁵⁵ developed a valuable algorithm to assess the *in vivo* 3D geometry of deformed stent-grafts, directly by x-ray projection, which would provide accurate clinical data.

Further works on the development of an AAA multimodality phantom may, thus, include a greater number of mechanobiological aspects, such as an atherosclerotic lesion, a more realistic intraluminal thrombus material, with porosity and calcifications.

V. CONCLUSION

In this study, a multimodality imaging phantom of a patient specific AAA geometry with fiducial markers and image features visible in MRA, CTA, DSA, and US has been developed. Another objective was to provide a visible realistic AAA thrombus in all tested modalities. Measurements of SNR and CNR values on T1 and T2 weighted sequences indicated reasonable agreement with reported values of human soft tissues *in vivo*. X-ray absorption was also in the range of HU numbers seen clinically for AAA scans. Ultrasound propagation speeds matched with the literature on phantoms and *ex vivo* biological tissues. This study also showed the feasibility of using this phantom to simulate fluoroscopy-guided stent graft deployment in a realistic AAA. Such simulation may help planning efficient endovascular intervention by improving stent development. However, future achievements should focus on better mimicking mechanical properties of AAA constituents.

ACKNOWLEDGMENTS

The authors acknowledge the contribution of Samir Merouche for measuring the speed of sound of the different phantom components, and François Treyve for his technical advice and help during the development and testing of the initial AAA phantom prototypes. This work was supported by Valorisation-Recherche Québec (Group Grant No. 2200-094) and by the Canadian Institutes of Health Research (Grant No. ISO-93328). G.C. and G.S. are former and present recipients of National Scientist awards of the Fonds de la Recherche en Santé du Québec.

^{a)} Author to whom correspondence should be addressed. Electronic mail: guy.cloutier@umontreal.ca

¹ M. P. Bergoeing, R. W. Thompson, and J. A. Curci, "Pharmacological targets in the treatment of abdominal aortic aneurysms," *Expert Opinion on Therapeutic Targets* **10**(4), 547–559 (2006).

² M. Prinssen, E. L. Verhoeven, J. Buth, P. W. Cuyppers, M. R. van Sambeek, R. Balm, D. E. Grobbee, and J. D. Blankensteijn, "A randomized trial comparing conventional and endovascular repair of abdominal aortic aneurysms," *N. Engl. J. Med.* **351**(16), 1607–1618 (2004).

³ T. A. M. Chuter, J. C. Parodi, and M. Lawrence-Brown, "Management of abdominal aortic aneurysm: A decade of progress," *J. Endovasc. Ther.* **11**(suppl II), II-82–II-95 (2004).

⁴ R. M. Greenhalgh, L. C. Brown, G. P. Kwong, J. T. Powell, and S. G. Thompson, "Comparison of endovascular aneurysm repair with open repair in patients with abdominal aortic aneurysm (EVAR trial) 30-day operative mortality results: Randomized controlled trial," *Lancet* **364**, 843–848 (2004).

⁵ R. M. Greenhalgh, L. C. Brown, J. T. Powell, S. G. Thompson, D. Epstein, and M. J. Sculpher, "Endovascular versus open repair of abdominal aortic aneurysm," *N. Engl. J. Med.* **362**(20), 1863–1871 (2010).

⁶ G. H. White, W. Yu, J. May, X. Chaufour, and M. S. Stephen, "Endoleak as a complication of endoluminal grafting of abdominal aortic aneurysms: Classification, incidence, and diagnosis," *Manage. J. Endovasc. Surg.* **4**(2), 152–168 (1997).

⁷ S. Lerouge, M.-C. Bonneviot, I. Salazkin, J. Raymond, and G. Soulez, "Endothelial denudation combined with embolization in the prevention of endoleaks after endovascular aneurysm repair: An animal study," *J. Endovasc. Therapy* **18**(5), 686–696 (2011).

⁸ R. M. Greenhalgh and J. T. Powell, "Endovascular repair of abdominal aortic aneurysm," *N. Engl. J. Med.* **358**, 494–501 (2008).

⁹ Z. Sun and T. Chaichana, "Fenestrated stent graft repair of abdominal aortic aneurysm: Hemodynamic analysis of the effect of fenestrated stents on the renal arteries," *Korean J. Radiol.* **11**(1), 95–105 (2010).

¹⁰ I. Avrahami, M. Brand, T. Meirson, Z. Ovadia-Blechman, and M. Halak, "Hemodynamic and mechanical aspects of fenestrated endografts for treatment of abdominal aortic aneurysm," *Eur. J. Mech. B/Fluids* **35**, 85–91 (2012).

¹¹ A. Prasad, N. Xiao, X.-Y. Gong, C. K. Zarins, and C. A. Figueroa, "A computational framework for investigating the positional stability of aortic endografts," *Biomech. Model Mechanobiol.* (in press).

¹² K. I. Paraskaeva, D. P. Mikhailidis, and D. Perrea, "Experimental models of abdominal aortic aneurysms: An overview," *Curr. Pharm. Des.* **14**(4), 325–337 (2008).

¹³ L. W. Tse, S. Lerouge, B. T. Bui, E. Therasse, H. Héon, and G. Soulez, "Radiofrequency perforation system for *in vivo* antegrade fenestration of aortic stent-grafts," *J. Endovasc. Ther.* **17**(2), 192–198 (2010).

¹⁴ G. Soulez, S. Lerouge, T. Darsaut, I. Salazkin, V. L. Oliva, and J. Raymond, "Role of the endothelial lining in endoleak formation and persistence after endovascular repair of aneurysm," *J. Vasc. Interv. Radiol.* **19**(7), 1070–1078 (2008).

¹⁵ R. A. Chaer, B. G. deRubertis, S. Trocciola, R. Hyneczek, S. C. Lin Russell, K. Lam, C. Kent, and P. L. Faries, "Basic science review: Characterization of endoleak following endovascular repair of abdominal aortic aneurysms," *Vasc. Endovasc. Surg.* **41**(2), 97–105 (2007).

- ¹⁶A. Sulaiman, C. Roty, J. M. Serfaty, C. Attia, L. Huet, and P. Douek, "In vitro, nonrigid model of aortic arch aneurysm, laboratory investigations," *J. Vasc. Interv. Radiol.* **19**(6), 919–924 (2008).
- ¹⁷P. Lermusiaux, C. Leroux, J. C. Tasse, L. Castellani, and R. Martinez, "Aortic aneurysm: Construction of a life-size model by rapid prototyping," *Ann. Vasc. Surg.* **15**(2), 131–135 (2001).
- ¹⁸N. Boussion, G. Soulez, J. de Guise, M. Daronat, Z. Qin, and G. Cloutier, "Geometrical accuracy and fusion of multimodal vascular images: A phantom study," *Med. Phys.* **31**(6), 1434–1443 (2004).
- ¹⁹L. Létourneau-Guillon, G. Soulez, G. Beauoin, V. L. Oliva, M. F. Giroux, Z. Qin, N. Boussion, E. Therasse, J. A. de Guise, and G. Cloutier, "CT and MR imaging of nitinol stents with radiopaque distal markers," *J. Vasc. Interv. Radiol.* **15**(6), 615–624 (2004).
- ²⁰V. Deplano, L. Bailly, and E. Bertrand, "Influence of blood shear-thinning behaviour on flow dynamics in abdominal aortic aneurysm *in vitro* compliant model," *Comput. Methods Biomech. Biomed. Eng.* **15**(suppl. 1), 49–52 (2012).
- ²¹K. Kato, T. Ishiguchi, K. Maruyama, S. Naganawa, and T. Ishigake, "Accuracy of plastic replica of aortic aneurysm using 3D-CT data for transluminal stent-grafting: Experimental and clinical evaluation," *J. Comput. Assist. Tomogr.* **25**(2), 300–304 (2001).
- ²²S. G. Lalka, S. M. Stockberger, M. S. Johnson, D. Hawes, A. Aisen, and S. O. Trerotola, "Phantom for calibration of preoperative imaging modalities in endoluminal stent-graft repair of aortic aneurysms," *J. Vasc. Interv. Radiol.* **9**(5), 799–807 (1998).
- ²³R. J. Winder, Z. Sun, B. Kelly, P. K. Ellis, and D. Hirst, "Abdominal aortic aneurysm and stent graft phantom manufactured by medical rapid prototyping," *J. Med. Eng. Technol.* **26**(2), 75–78 (2002).
- ²⁴P. E. Baker and K. V. Ramnarine, "Development and application of an experimental abdominal aortic aneurysm model," *Br. Med. Ultrasound Soc.* **17**(1), 30–34 (2009).
- ²⁵E. Berry, A. Marsden, K. W. Dalgarno, D. Kesser, and D. J. A. Scott, "Flexible tubular replicas of abdominal aortic aneurysms," *Proc. Inst. Mech. Eng., Part H: J. Eng. Med.* **216**(11), 211–214 (2002).
- ²⁶W. Mower, W. Quiñones, and S. Gambhir, "Effect of intraluminal thrombus on abdominal aortic aneurysm wall stress," *J. Vasc. Surg.* **26**(4), 602–608 (1997).
- ²⁷E. A. Van Dam, S. D. Dams, G. W. M. Peters, M. C. M. Rutten, G. W. H. Schurink, J. Buth, and F. N. van de Vosse, "Determination of linear viscoelastic behaviour of abdominal aortic aneurysm thrombus," *Biorheology* **43**, 695–707 (2006).
- ²⁸S. S. Hans, O. Jareunpoon, M. Balasubramaniam, and G. B. Zelenock, "Size and location of thrombus in intact and ruptured abdominal aortic aneurysms," *J. Vasc. Surg.* **41**(4), 584–588 (2005).
- ²⁹L. Allard, G. Soulez, B. Chayer, F. Treyve, Z. Qin, and G. Cloutier, "Multimodality vascular imaging phantoms: A new material for the fabrication of realistic 3D vessel geometries," *Med. Phys.* **36**(8), 3758–3763 (2009).
- ³⁰G. Cloutier, G. Soulez, S. Qanadli, P. Teppaz, L. Allard, Z. Qin, F. Cloutier, and L. G. Durand, "A multimodality vascular imaging phantom with fiducial markers visible in DSA, CTA, MRA and ultrasound," *Med. Phys.* **31**(6), 1424–1433 (2004).
- ³¹R. Brown, *Physical Testing of Rubber*, 4th ed. (Springer, New York, 2006).
- ³²E. L. Madsen, F. Dong, G. R. Frank, B. S. Garra, K. A. Wear, T. Wilson, J. A. Zagzebski, H. L. Miller, K. K. Shung, S. H. Wang, E. J. Feleppa, T. Liu, W. D. O'Brien, K. A. Topp, N. T. Sanghvi, A. V. Zaitsev, T. J. Hall, J. B. Fowlkes, O. D. Kripfgans, and J. G. Miller, "Interlaboratory comparison of ultrasonic backscatter, attenuation, and speed measurements," *J. Ultrasound Med.* **18**, 615–631 (1999).
- ³³I. Y. Kuo, B. Hete, and K. K. Shung, "A novel method for the measurement of acoustic speed," *J. Acoust. Soc. Am.* **88**(4), 1679–1682 (1990).
- ³⁴J. D. Brown, J. Rosen, Y. S. Kim, L. Chang, M. N. Sinanan, and B. Hannaford, "In-vivo and in-situ compressive properties of porcine abdominal soft tissues," *Stud. Health Technol. Inform.* **94**, 26–32 (2003).
- ³⁵J. H. Ashton, J. P. VandeGeest, B. R. Simon, and D. G. Haskett, "Compressive mechanical properties of the intraluminal thrombus in abdominal aortic aneurysms and fibrin-based thrombus mimics," *J. Biomech.* **42**, 197–201 (2009).
- ³⁶R. Frayne, L. M. Gowman, D. W. Rickey, D. W. Holdsworth, P. A. Picot, M. Drangova, K. C. Chu, C. B. Caldwell, A. Fenster, and B. K. Rutt, "A geometrically accurate vascular phantom for comparative studies of x-ray, ultrasound, and magnetic resonance vascular imaging: Construction and geometrical verification," *Med. Phys.* **20**(2), 415–425 (1993).
- ³⁷W. Dabrowski, J. Dunmore-Buyze, R. N. Rankin, D. W. Holdsworth, and A. Fenster, "A real vessel phantom for imaging experimentation," *Med. Phys.* **24**, 687–693 (1997).
- ³⁸S. A. P. Cornelissen, H. J. M. Verhagen, J. A. van Herwaarden, E. P. A. Vonken, F. L. Moll, and L. W. Bartels, "Lack of thrombus organization in non-shrinking aneurysms years after endovascular abdominal aortic aneurysm repair," *J. Vasc. Surg.* **56**, 938–942 (2012).
- ³⁹M. Castrucci, R. Mellone, A. Vanzulli, A. De Gaspari, R. Castellano, D. Astore, R. Chiesa, A. Grossi, and A. Del Maschio, "Mural thrombi in abdominal aortic aneurysms: MR imaging characterization – Useful before endovascular treatment," *Radiology* **197**, 135–139 (1995).
- ⁴⁰C. M. Kramer, L. A. Cerilli, K. Hagspiel, J. M. DiMaria, F. H. Epstein, and J. A. Kern, "Magnetic resonance imaging identifies the fibrous cap in atherosclerotic abdominal aortic aneurysm," *Circulation* **109**, 1016–1021 (2004).
- ⁴¹A. Nchmi, O. Defawe, D. Brisbois, T. K. Y. Broussaud, J. O. Defraigne, P. Magotteaux, B. Massart, J. M. Serfaty, X. Houard, J. B. Michel, and N. Sakalihasan, "MR imaging of iron phagocytosis in intraluminal thrombi of abdominal aortic aneurysms in humans," *Radiology* **254**(3), 973–981 (2010).
- ⁴²J. T. Bushberg, J. A. Seibert, E. M. Leidholdt, Jr., and J. M. Boone, *The Essential Physics of Medical Imaging*, 2nd ed. (Lippincott Williams and Wilkins, Philadelphia, 2002).
- ⁴³T. Yoshizumi, T. Nakamura, M. Yamane, A. Hasan, M. Menju, K. Yamasaki, T. Arai, K. Kotani, T. Funahashi, S. Yamashita, and Y. Matsuzawa, "Abdominal fat: Standardized technique for measurement at CT," *Radiology* **211**, 283–286 (1999).
- ⁴⁴W. D'Souza, E. L. Madsen, O. Unal, K. K. Vigen, G. R. Frank, and B. R. Thomadsen, "Tissue mimicking materials for a multi-imaging modality prostate phantom," *Med. Phys.* **28**(4), 688–700 (2001).
- ⁴⁵K. Tokunaga and H. Hanaizumi, "Extraction of the thoracic aorta territory and aneurysm from CT images," *SICE Annual Conference in Sapporo, Japan, 4–6 August* (IEEE Conference Publication, 2004), Vol. 3, pp. 2188–2192.
- ⁴⁶H. Tomoda, M. Hoshiai, A. Tagawa, R. Tagawa, S. Koide, S. Kawada, A. Shotsu, and S. Matsuyama, "Evaluation of left atrial thrombus with computed tomography," *Am. Heart J.* **100**(3), 306–310 (1980).
- ⁴⁷J. Roy, F. Labruto, M. O. Beckman, J. Danielson, G. Johansson, and J. Swedenborg, "Bleeding into the intraluminal thrombus in abdominal aortic aneurysms is associated with rupture," *J. Vasc. Surg.* **48**, 1108–1113 (2008).
- ⁴⁸B. A. Bullen, F. Quaade, E. Olesen, and S. A. Lund, "Ultrasonic reflections used for measuring subcutaneous fat in humans," *Human Biol.* **37**, 375–384 (1965).
- ⁴⁹J. A. Rooney, P. M. Gammeli, J. D. Hestenes, H. P. Chin, and D. H. Blankenhorn, "Velocity and attenuation of sound in arterial tissues," *J. Acoust. Soc. Am.* **71**(2), 462–466 (1982).
- ⁵⁰H. TenHoff and J. D. Koger, "Ultrasound transducer with extended focus," patent number 5,984,871 (November 16, 1999).
- ⁵¹C. K. Chung, T. V. How, and P. L. Harris, "Flow visualization in a model of a bifurcated stent-graft," *J. Endovasc. Ther.* **12**(4), 435–445 (2005).
- ⁵²M. Gwenda, P. Knez, S. Winter, G. Jaschke, G. Wassmer, T. Schmitz-Rixen, and J. Brunkwall, "Endotension is influenced by wall compliance in a latex aneurysm model," *Eur. J. Vasc. Endovasc. Surg.* **27**(1), 45–50 (2004).
- ⁵³T. J. Corbett, A. Callanan, L. G. Morris, B. J. Doyle, P. A. Grace, E. G. Kavanagh, and T. M. McGloughlin, "A review of the in vivo and in vitro biomechanical behaviour and performance of postoperative abdominal aortic aneurysms and implanted stent-grafts," *J. Endovasc. Ther.* **15**(4), 468–484 (2008).
- ⁵⁴T. J. Corbett, B. J. Doyle, A. Callanan, M. T. Walsh, and T. M. McGloughlin, "Engineering silicone rubbers for in vitro studies: Creating AAA models and ILT analogues with physiological properties," *J. Biomech. Eng.* **132**(1), 011008 (2009).
- ⁵⁵S. Demirci, A. Bigdelou, W. Lejing, C. Wachinger, M. Baust, R. Tibrewal, R. Ghotbi, H. H. Eckstein, and N. Navab, "3D stent recovery from one x-ray projection," *Med. Image Comput. Comput. Assist. Interv.* **14**(Pt 1), 178–185 (2011).